Earth Planet. Sci. Lett. 679 (2026) 119891

Contents lists available at ScienceDirect

Earth and Planetary Science Letters

journal homepage: www.elsevier.com/locate/epsl

Interannual to multidecadal climate oscillations occurred during Cryogenian glaciation

Chloe Griffin [a,*], Thomas M. Gernon [a,b], Minmin Fu [a], Elias J. Rugen [a], Anthony M. Spencer [c], Geoffrey Warrington [d], Thea K. Hincks [a]

[a] School of Ocean and Earth Science, University of Southampton, Southampton SO14 3ZH, United Kingdom
[b] GFZ Helmholtz Centre for Geosciences, 14473 Potsdam, Germany
[c] Madlavollveien 14, 4041, Hafrsfjord, Norway
[d] School of Geography, Geology and the Environment, University of Leicester, Leicester, LE1 7RH, United Kingdom

ARTICLE INFO

Editor: Dr H Bao

Keywords:
Varves
Paleoclimate
Cryogenian
Solar cycle
Climate cycle

ABSTRACT

During the two Cryogenian snowball Earth glaciations, the Sturtian (ca. 717–658 Ma) and Marinoan (ca. 639–635 Ma), ice persisted in the tropics for millions of years. Previous analyses of varves deposited before and after these glaciations have revealed climate variability linked to solar, oceanic, and atmospheric dynamics. However, to our knowledge, no evidence of sub-Milankovitch scale climatic variability has been documented during the glaciations themselves. The proposition of reduced solar luminosity in the Cryogenian, an attenuated hydrological cycle, and an expected hiatus in atmosphere-ocean interactions due to ocean freezing, raises questions regarding whether solar-ocean-atmospheric interactions continued during these glaciations. We analyze a unit of 2,640 laminites within the Sturtian Port Askaig Formation on the Garvellach Islands, Scotland, to better understand climate variability during a discrete interval of the Sturtian. Our study indicates the laminites most likely represent annual varves, reflecting seasonal freeze-thaw cycles in a deep, quiescent waterbody. Spectral analysis of laminae thickness reveals decadal and centennial periodicities consistent with present-day Schwabe and Gleissberg solar cycles, alongside interannual periodicities, likely tied to ocean-atmospheric climate modes, resembling the modern El-Niño Southern Oscillation. Our coupled Cryogenian climate simulations under varying degrees of ice coverage produce similar interannual periodicities in surface temperatures near the paleo-coordinates of the Garvellach Islands and in the tropics. This evidence reveals that solar-ocean-atmospheric interactions generated a wider range of climatic variability than expected during snowball Earth and hints at the possibility of transient unfrozen tropical waters during the Sturtian, or other yet unexplored modes of internal climate variability.

1. Introduction

The degree to which Earth's climate retained seasonality and ocean-atmospheric coupling during the Cryogenian period remains uncertain. Under snowball Earth conditions, one classic hypothesis envisions a planet entirely encased in ice with a largely quiescent hydrological cycle (Hoffman et al., 1998). However, other observational and modelling constraints imply that open water persisted to some degree in the tropics, which may permit ocean-atmospheric coupling and reconcile photosynthetic survival with low-latitude glacial activity (Abbot et al., 2011; Hyde et al., 2000; Le Heron et al., 2011). The Sturtian, the older and longer of these glaciations, is documented worldwide by thick, glaciogenic successions. Field data (e.g., polygonal sand wedges and freeze-thaw structures) and numerical modelling highlight the persistence of strong seasonal temperature contrasts (Deynoux, 1982; Hoffman and Li, 2009; Spencer, 1971) as extreme continentality and low thermal inertia may have amplified seasonality, especially at low paleolatitudes (Hoffman et al., 2017; Liu et al., 2020; Williams, 2008), generating pronounced freeze-thaw cycles. Understanding how seasonality and hydrological cycling operate under near-fully glaciated conditions is an important climate question with key biological implications.

Annually laminated, or varved (after De Geer, 1912), sediments offer unique means of addressing these questions as they represent

* Corresponding author.
E-mail address: c.griffin@soton.ac.uk (C. Griffin).

https://doi.org/10.1016/j.epsl.2026.119891
Received 12 November 2025; Received in revised form 24 January 2026; Accepted 27 January 2026
Available online 4 February 2026

high-resolution records of paleoenvironmental change, capturing variations in climate-driven processes (Brauer, 2004). In glacial environments, varve thickness reflects a range of environmental controls that drive seasonal variations in meltwater production, sediment supply and hence varve thickness. These include both internal dynamics within the glacio-hydrological system (Desloges and Gilbert, 1994) and external forcing (e.g., climatically driven sediment flux variations) (De Geer, 1908; Zolitschka et al., 2015). Firstly, sediment flux and hence varve thickness may be driven by intermittent sediment storage and release within the glacio-hydrological system, generating natural variability in sediment flux in the absence of external forcing. This means that varve thickness may record the temporal variability in the ability of glacially conditioned sediment to be mobilized and transported by ice and meltwater (Antoniazza and Lane, 2021). However, in periglacial or glacial environments, variations in ice extent are commonly driven by climatic variability that influences glacier mass balance and advance-retreat cycles (Palmer et al., 2019), allowing varve thickness to be utilized as a paleoclimate proxy (De Geer, 1912; Ojala et al., 2012; Zolitschka et al., 2015).

Alongside the annual cycle, the potential of varves to record interannual to centennial climatic oscillations has been demonstrated (e.g., Dean et al., 2002; Hasegawa et al., 2022; Howe et al., 2016). Climate drivers, such as solar irradiance, ocean-atmospheric circulation patterns and aerosol-cloud interactions influence global temperature, precipitation, wind patterns and weathering intensity. These modulate freeze-thaw cycles and erosion, thereby controlling varve deposition across short and long periods (Lafond et al., 2023). Over decadal to centennial timescales, solar irradiance variations, for instance, the Schwabe cycle (9–16 years; Miyake et al., 2013) and Gleissberg cycle (60–150 years; Usoskin and Mursula, 2003) generate subtle variations in global temperatures (Reid, 2000) that modulate glacial dynamics and sedimentation. The Schwabe cycle is well documented in many proxies over the Holocene and is the most common periodicity recorded in varves throughout geological time, with minimal variability in periodicity from the Quaternary (Amann et al., 2015; Lafond et al., 2023) to the Proterozoic (Andrews et al., 2010; Howe et al., 2016; Hughes et al., 2003; Shatsillo et al., 2019). Dust aerosol-cloud interactions can also impact global climate on decadal timescales both independently and through interactions with solar radiation. However, these complex atmospheric feedbacks remain large sources of uncertainty in estimates of climate sensitivity (Van De Koot et al., 2025). Over shorter timescales, well-documented multiannual climate oscillations such as the Quasi-Biennial Oscillation (QBO) and El-Niño Southern Oscillation (ENSO), cause a global redistribution of temperature, precipitation, and ocean-atmospheric circulation patterns, with present day periodicities of 2–3 years and 3–7 years, respectively (McPhaden et al., 2006). While changes in paleogeography and global temperatures undoubtedly caused the period and intensity of these oscillations to vary through time, proxy and model evidence suggest ENSO has been robust for at least the past several hundred millions of years (Gao et al., 2025; Huber and Caballero, 2003; Li et al., 2024).

Although the mechanisms of climate variability are well documented today, the number of records thought to reflect annual resolution decreases considerably with geological age, limiting understanding of past climatic variability (Andrews et al., 2010). Whilst evidence from banded iron formations suggests that Milankovitch-scale orbital forcing remained a key driver of ice sheet dynamics during snowball Earth (Mitchell et al., 2021), definitive evidence for interannual to (multi) decadal climate variability, especially from internal climate modes involving coupled ocean-atmospheric dynamics, remains undocumented. Sunspot cyclicity has been inferred from varves both before (Hughes et al., 2003; Li et al., 2018; Tang et al., 2014) and after (Andrews et al., 2010; Korn and Martin, 1951) the Sturtian. Notwithstanding this, external forcing mechanisms likely persisted during the Cryogenian, but whether the effects of this surface forcing were dampened by extensive ice cover remains uncertain. More critically, definitive evidence for internal climatic variability during snowball Earth remains scarce. Ocean-atmospheric climate patterns analogous to the modern day are contingent on the presence of open-ocean. As the extent of sea ice throughout the Cryogenian remains uncertain, the existence and degree of ocean-atmospheric coupling during the Sturtian is unresolved. Consequently, questions remain regarding whether internal climate cycles could operate during snowball Earth, and if so, what their expression reveals about the extent of open-ocean and the dynamics of the Cryogenian climate system.

Cryogenian deposits generally constitute chaotic glacial diamictites, and varved sediments remain rare (Benn et al., 2015; Le Heron et al., 2011). However, rhythmically laminated sediments of Sturtian age have been described from the Port Askaig Formation on the Garvellach Islands, Scotland (Fig. 1), and previously suggested to represent annual varves (Spencer, 1971). Despite this, the origin of these laminites remains uncertain, and periodicity in laminae thickness has not been detected.

To investigate solar and climate cycles during the Sturtian, we conducted sedimentological and spectral analyses of the D32 laminite bed (hereafter, laminites for brevity), within the Port Askaig Formation. We characterize these laminites, evaluate their depositional origin and infer that deposition was strongly influenced by seasonal variations. Using spectral analysis, we interpret thickness variations to reflect sedimentological cyclicity linked to interannual to centennial solar and climate oscillations. Our interpretation of the varve record is guided by comparison to our climate model simulations of the Sturtian glaciation under three different ice coverage scenarios. Our findings suggest that these laminites provide a rare and unique record of a sustained hydrological cycle and climatic variability during this discrete interval of the Sturtian, revealing that solar-climate coupling may have continued unabated during this time interval either due to the existence of unfrozen tropical water, or yet unexplored modes of internal climate variability.

2. Geological setting

The Port Askaig Formation is exposed across Scotland and Ireland, notably on the Isle of Islay and the Garvellach Islands (Spencer, 1971) (Fig. 1). The Formation marks the base of the Argyll Group within the Dalradian Supergroup, deposited between the Tonian (~840 Ma) and early Ordovician (~510 Ma) (Fairchild et al., 2018). The Port Askaig Formation is assigned to the Sturtian glaciation based on lithostratigraphy as well as carbon and strontium isotope chemostratigraphy (Fairchild et al., 2018). This is also consistent with maximum depositional U-Pb ages from detrital zircon grains throughout the formation (Fig.1) (Rugen et al., 2024).

The Port Askaig Formation records a dynamic, low latitude, glacial system during the Cryogenian, where at the time the Garvellach Islands lay around 30°S. The Formation is subdivided into 5 members (Spencer, 1971), containing 48 discrete, numbered diamictite units interbedded with sandstone, siltstone, and mudstone, documenting the repeated, perhaps orbitally controlled, advance and retreat of ice throughout deposition (Ali et al., 2018).

The laminite bed outcrops on Garbh Eileach (56.2°N, 5.6°W), within Member 2 of the Port Askaig Formation and occurs 12 m above Diamictite 32 (D32) and 350 m from the base of the Formation (Fig. 1). Given the age of the Port Askaig Formation, the laminites represent a discrete interval of the Sturtian, with a maximum depositional age of 687 ± 10.3 Ma, constrained by a single detrital zircon U-Pb age (Rugen et al., 2024).

3. Materials and methods

3.1. Field measurements

Field measurements of couplet thickness (light, coarse-grained and dark, fine-grained laminae) were collected from the D32 laminites

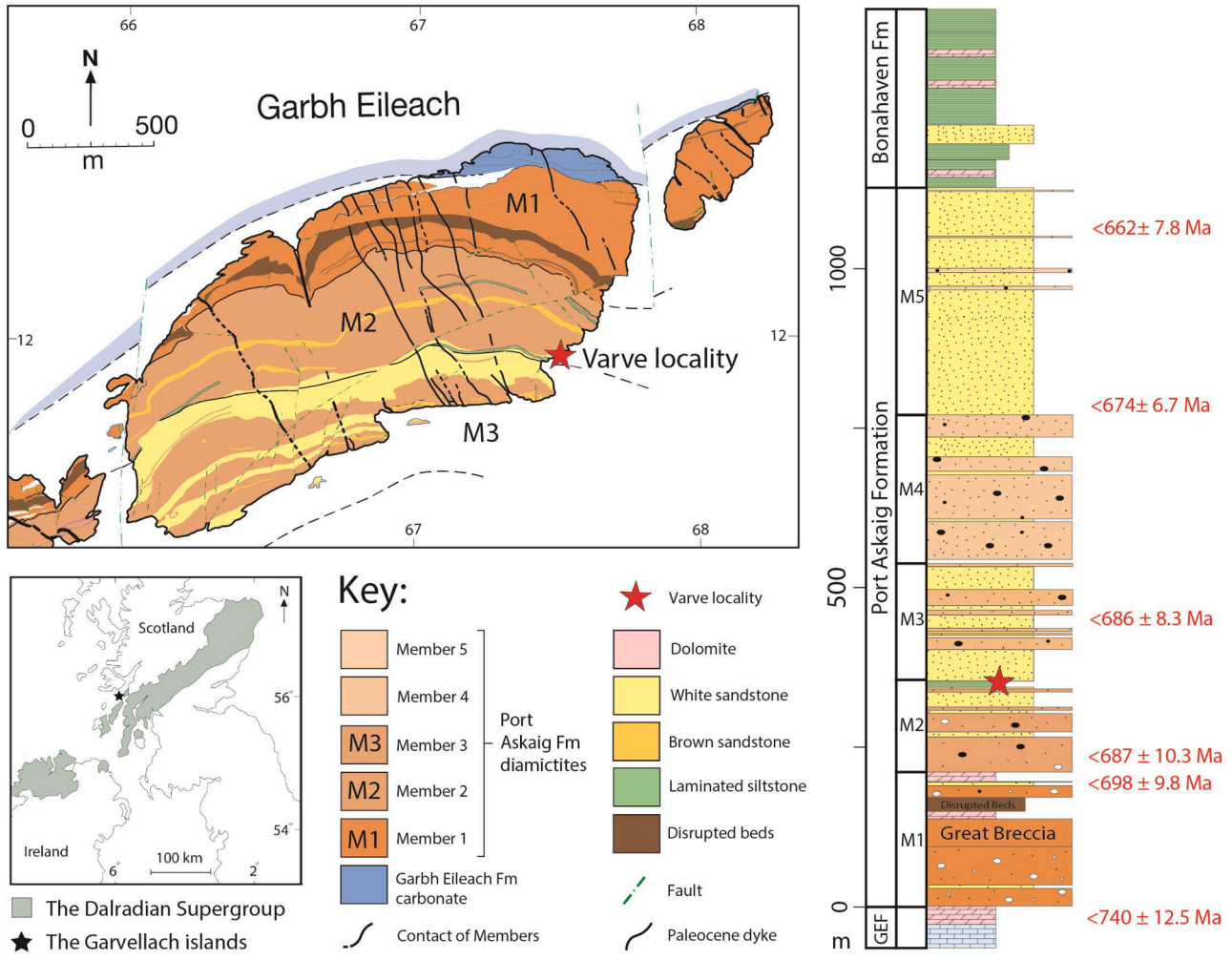

Fig. 1. Geological map of Garbh Eileach, the largest of the Garvellach Islands, with the location of the D32 laminites highlighted with a star. The laminites occur at the top of Member 2 (M2) of the Port Askaig Formation, a glaciogenic succession within the Dalradian Supergroup. Age constraints derived from youngest detrital zircon U-Pb ages are provided throughout the Port Askaig Formation (Rugen et al., 2024).

(Fig. 18, Spencer, 1971) by marking the base of each lamina onto tracing film directly from the outcrop. The tracing film documenting these measurements and a scale bar were scanned and digitized in MATLAB, generating a ~5.5 m thickness series, containing 2640 discrete laminae (Fig. 2B). A sample was taken from the middle of the outcrop and made into thin sections (Fig. 3 and 4), which were analyzed under both plane and cross-polarized light using an Olympus BX-60 petrographic microscope and imaged using a Canon-EOS-60D camera. Photomicrographs were stitched together using Autopano Giga (Kolor ©) Software (Fig. 4).

3.2. Time series analysis

To determine the presence of sedimentological cyclicity within the laminites, power spectral analysis was conducted in Acycle 2.8 (Li et al., 2019). Firstly, the laminae thickness series was detrended to remove excessive low frequency components, then the classic multi-taper method (MTM) (Thomson, 1982) was used to obtain the spectrum. This was conducted in the stratigraphic domain using a bed-number series of laminae thickness, providing an interpolation-free depth series. The statistical significance of spectral peaks was tested relative to the null hypothesis (e.g., no external forcing) of a red noise background, using the classic AR(1) model, at confidence levels of 95 %, 99 % and 99.9 %. This produced a set of spectral peaks representing cycles per laminae, which were converted into the time domain.

To determine the stationarity of the laminae thickness series, the moving variance was computed using a sliding window of 500 laminae. Subsections of time series are commonly used to mitigate distortions caused by abrupt changes in sedimentation rate, thereby producing the stationarity required to avoid spectral smearing and peak splitting (Weedon et al., 2019). As the variance is high for the lowermost half of the time series (Fig. 2B), MTM power spectra were computed for the full laminae thickness series, alongside both halves of the thickness series (n = 1320 laminae). Here, the upper 1320 laminae, where the mean and variance of the data remain essentially constant, may be interpreted as a more useful description of the time series (Weedon, 2003).

To investigate the stratigraphic changes in the occurrence of regular cyclicity, an evolutionary power spectrum was used. The evolutionary spectrum was generated in Acycle 2.8, using the MTM method, and was calculated using a sliding window of 300 laminae. Here, contours of high-power indicate stratigraphically persistent, regular cyclicity.

3.3. Uncertainty assessment

To reduce uncertainty during the measurements of varve thickness from the outcrop, measurements were taken on a stepped transect (Fig. 3A), to target faces consistently normal to bedding. As the dip of the strata does not vary much over the ~5.5 m section, any apparent dip effects would lead to systematic uncertainty in varve thickness over the entire thickness series. Nevertheless, to account for random errors associated with the interpretation and measurement of laminae

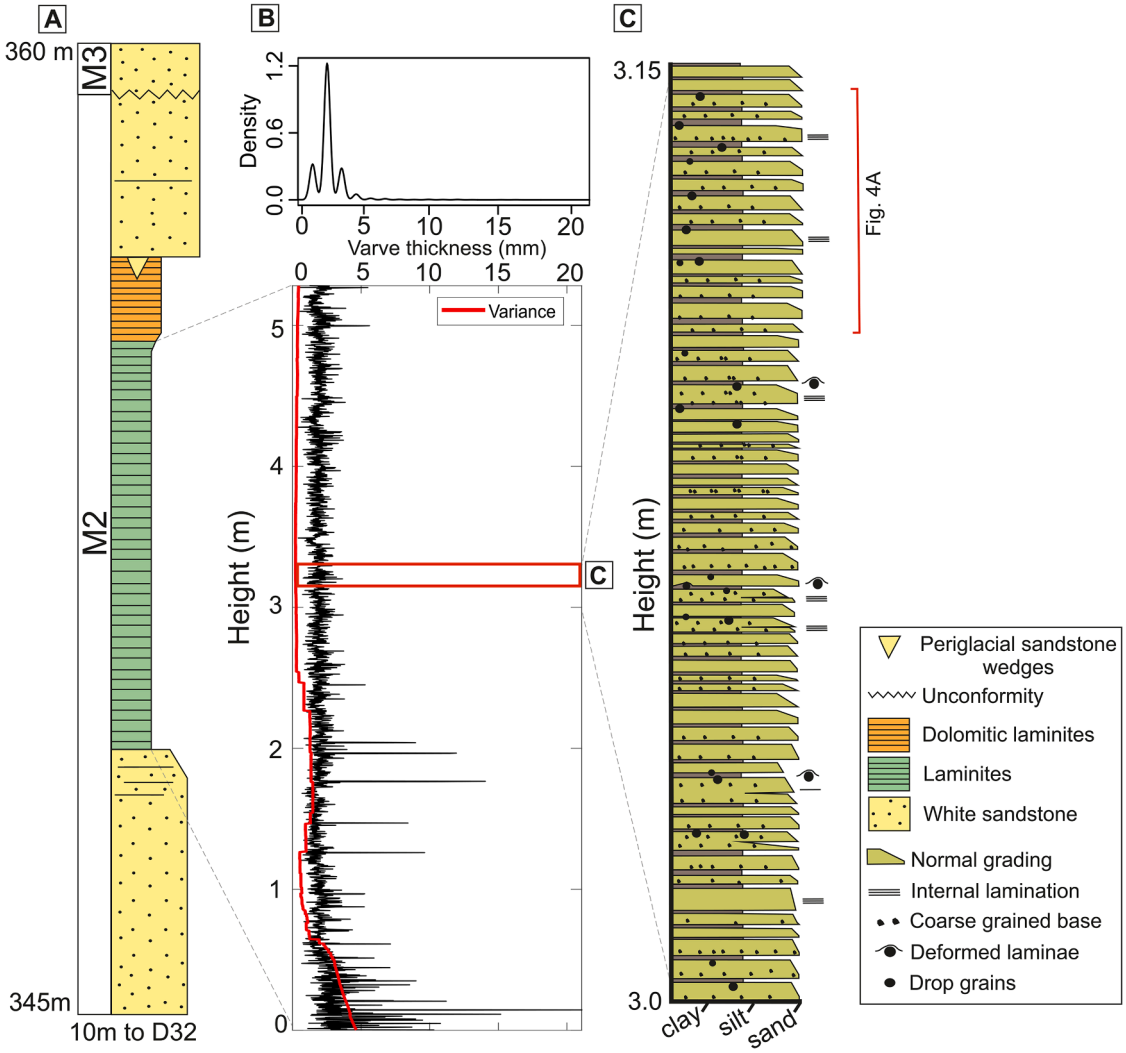

Fig. 2. (A) Stratigraphic column showing 15 m of strata at the top of Member 2 (M2) of the Port Askaig Formation (Fig. 1). (B) D32 laminae thickness series and moving variance of the thickness series (window = 500 laminae) (C) Schematic sedimentary log made from the sample and overlapping thin sections, showing the representative characteristics of the laminae in part of the outcrop.

thickness, the recording of these onto paper and during the digitizing process, 1000 different thickness series were generated, varying each thickness by the estimated uncertainty of ±1 mm using a beta distribution. Power spectra were generated for each iteration for the full time series and both halves of the thickness series. The average power of each signal spike exceeding the 99 % confidence level over 1000 iterations was calculated and compared to the power of the 99 % and 95 % confidence levels at the signal periodicity to quantify the variability in signal detectability (Supplementary Material; Fig. S1, Table S1).

3.4. Climate modelling

To understand the occurrence and operation of interannual climate oscillations during the Sturtian, we perform simulations of 720 Ma conditions using the Community Earth System Model (CESM) version 1.2.2 in a fully coupled atmosphere-ocean configuration. CESM uses the Community Atmosphere Model version 5 (CAM5) as its atmospheric component (Neale et al., 2012) and Parallel Ocean Program version 2 as its ocean component (Danabasoglu et al., 2012).

The Neoproterozoic simulations used 720 Ma paleogeography from the reconstruction of Merdith et al. (2021); the paleogeography was manually modified to avoid small channels and bays which can lead to numerical instability. A circular orbit with zero eccentricity and 23.5° obliquity was used, and solar insolation was set to 94 % of the present day. Trace gases were maintained at preindustrial levels. The resolution of the model is 3.75° in the atmosphere and a nominal 3° in the ocean.

Three snowball Earth scenarios were evaluated using different background CO_2 concentrations to understand how sea ice extent influences the frequencies present in the power spectra; no land ice is present in the simulations. The three scenarios include: 5 ppm, replicating a hard snowball Earth with 99 % sea ice coverage, 10 ppm, replicating a scenario with a equatorial oasis with 85 % sea ice coverage, and 100 ppm, replicating a waterbelt Earth allowing open water circulation at the equator with 60 % sea ice coverage. The hard snowball scenario uses a 50 m mixed layer ocean and no prescribed ocean heat transport to ensure numerical stability. The other two scenarios were run fully coupled with a dynamic ocean.

The 5 ppm, 10 ppm, and 100 ppm simulations were spun up for 100, 500, and 700 years respectively, until sea ice coverage and global energy balance had equilibrated. They were then integrated for an additional 1000 years; the period that was used for our analysis. We output the global distribution of annual-mean surface temperature over 1000 years for each scenario, allowing the identification of annual to multidecadal periodicities. Below, we present evidence supporting the interpretation that these laminae most likely represent annual varves, hence the model data was converted from its default monthly output to annual-mean

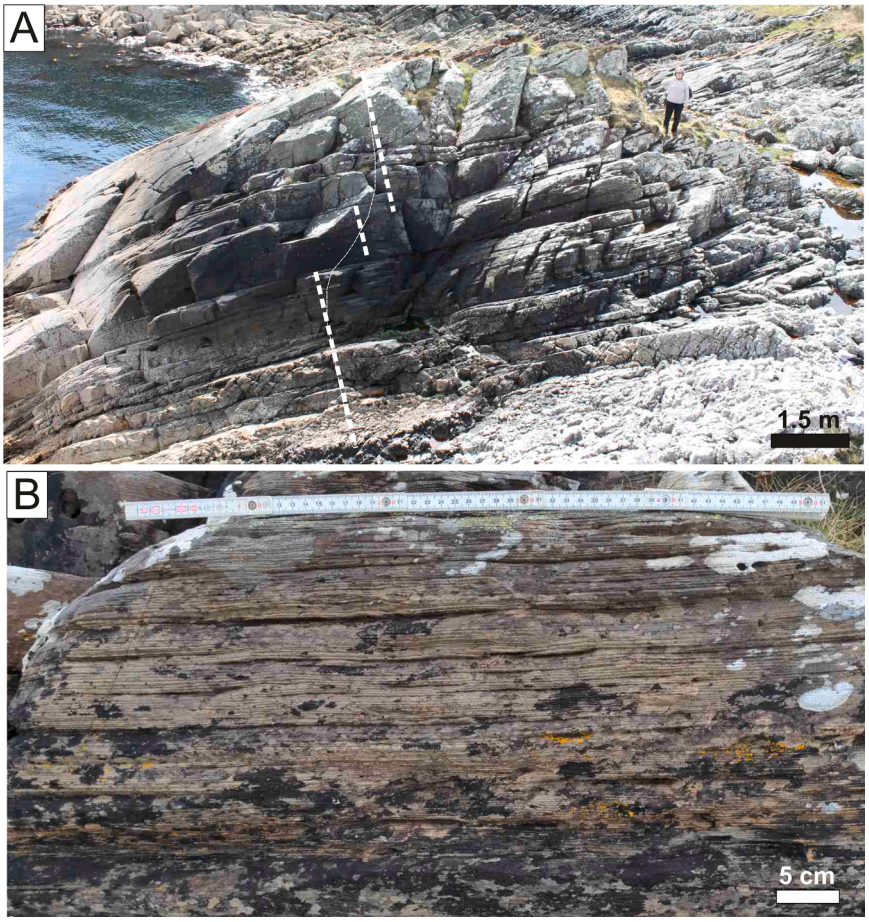

Fig. 3. (A) Outcrop photograph of the D32 laminites locality showing the approximate location where the laminae were measured (white dashed line). (B) Field photograph of the laminites (looking south).

surface temperatures to allow direct comparison to the laminite thickness series.

Firstly, to quantify temperature variability at the study site, the coordinates of the Garvellach Islands during the Sturtian glacial interval (30.6S, 145.6E) were obtained using the reconstruction of Merdith et al. (2021), and a time series of annual surface temperature was extracted from this location for each simulation (Fig. S3; Supplementary Material). To understand the sensitivity of the power spectra to paleogeographic location and to ensure the signals present at the study site are representative per scenario, annual mean surface temperatures were extracted from a 5 × 5 grid of cells (~600 km radius) around the coordinates of the study site per scenario (Fig. S4; Supplementary material). Secondly, to quantify interannual variability in the tropics driven by ocean circulation patterns, a 60° longitude and 10° latitude box was defined in an equatorial region containing open water in two of the scenarios (5°S-5°N, 67.5°W-7.5°W). The mean annual surface temperature in this region was calculated from 64 individual time series (Fig. S3; Supplementary Material). Power spectral analysis was also conducted in Acycle 2.8 (Li et al., 2019), using the same method as applied to the laminite thickness series. Frequencies above the 95 %, 99 % and 99.9 % confidence levels were considered statistically significant.

4. Results

4.1. Characteristics of the laminites

In outcrop, the laminites are densely packed with a laterally continuous, plane-parallel lamination structure; no variation in outcrop-scale sedimentary structure was observed vertically or laterally across the outcrop (Fig. 3A-B). In general, the laminae bases are sharp and planar with no discernible evidence of erosive surfaces. The laminae thicknesses range from 0.3 to 21 mm; the thickest laminae are in the lowermost meter of the section, and laminae thickness decreases over the first 2.5 m, after which the variability in laminae thickness reduces (Fig. 2B).

Microscopically, the most pronounced feature is the consistent presence of sharply defined light and dark colored laminae, where the light laminae are consistently thicker than the dark laminae (Fig. 4A). A weak internal lamination is evident halfway through some of the light laminae. The light laminae are composed of well-sorted, subangular grains which show normal grading from fine sand to silt. There is a sharp but non-erosive upper contact to the thin, dark laminae, which are composed of silt and clay and show no discernible grading. Medium to coarse subangular grains (Fig. 4B), which are anomalously large in relation to the matrix (0.5–1.5 mm diameter), are present throughout the laminites. These larger grains are present in every lamina with variable abundance (Fig. 4C), and generally mark the base of the light laminae, displacing the dark laminae below. Coarse grains are rarely found within the dark laminae (Fig. 4C); however, they can be found sporadically at the sharp upper contact, often displacing the overlying dark laminae.

4.2. Time series analysis of the laminites

Due to the change in variance throughout the time series, spectral analysis was conducted on the entire thickness series (Fig. 5A), as well as both halves of the thickness series (Fig. 5B-C). An evolutionary power spectrum was plotted to assess the stationarity of identified cyclicity

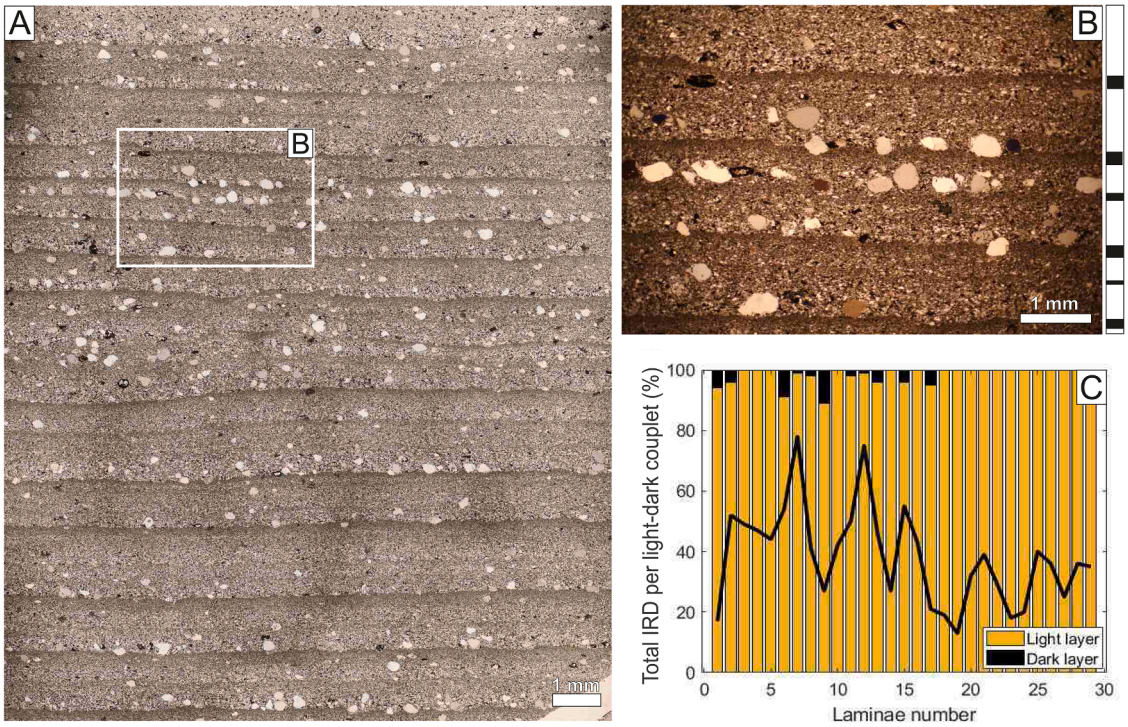

Fig. 4. (A) Thin section photomicrograph in plane polarized light documenting the fine-scale internal structure of the laminations. (B) A thin section photograph in cross polarized light of four laminae (white box in A); laminae couplets generally comprise coarse-grained (light) lower and fine-grained (dark) upper layers, indicated by the white and black bars, respectively. The base of the light laminae is marked by medium to coarse quartz grains. (C) Point count data of the anomalously large quartz grains within each light-dark couplet showing both total coarse grain count per couplet (black line) and the percentage of coarse grains within the light and dark layers respectively (yellow and black bars).

through the 5.5 m section (Fig. 5D).

Time series analysis of the complete thickness series of 2,640 laminae (Fig. 5A) reveals a range of prominent peaks between the 95 % and 99.9 % confidence levels (Table 1). Above the 99.9 % confidence level, prominent peaks at 2.1, 2.2, 3.1 and 4.2 laminae are evident. At the 99 % confidence level, peaks are evident at 2.4, 2.5, 2.7, 5.2, 16.9, 48 and 138 laminae and at the 95 % confidence level, peaks at 3.2, 3.5, 4.2–4.5, 6.2–6.3, 9 and 11 laminae are evident.

In the evolutionary power spectrum (Fig. 5D), the most persistent cycles are approximately 4–4.5, 9, 13.7–16.9 and 130–150 laminae, with the cycles at 9 and 135–150 laminae exhibiting the highest consistent power. The onset of these persistent cycles generally coincides with a marked reduction in variance at 0.5 m from the base of the laminites (Fig.2B). Whilst frequencies in the range of 4–4.5, 8–9 and 17–13 laminae are evident in all three power spectra confirming their persistence, the patterns evident in the evolutionary power spectrum are best represented by the power spectrum of the top 1320 laminae (Fig. 5B). Here, these persistent periodicities increase in detectability to be evident at the 99–99.9 % confidence levels. This is likely because the variance is very low, allowing strongly periodic components to be more robustly identified. Periodicity between 2–4 laminae is also evident but is less persistent throughout the entire section. Although non-stationary, these frequencies are evident in all three power spectra above the 95 % confidence level and occur in parts of the evolutionary power spectra (0.25 – 1.25 m and 2.5 – 4 m) with significant power (Fig. 5D).

4.3. Time series analysis of modelled surface temperature

Simulated annual surface temperature at the paleo-coordinates of the Garvellach Islands and in the tropics (defined by the 60° longitude and 10° latitude box) from all three modelled scenarios reveals a range of prominent peaks between the 95 % and 99 % confidence levels (Fig. 6B-D, Fig. 7; Table 1).

At both the Garvellach Islands and in the tropics, all three scenarios reveal peaks between 2 and 3 years above at least the 95 % confidence level. In the tropics, both the hard snowball and waterbelt scenarios contain peaks at the 99.9 % confidence level at 2.6 and 2.7 years. . At the Garvellach Islands, the two scenarios with open-ocean contain frequencies between 3.2 and 5.4 years at the 95 % and 99 % confidence levels, but this large range of frequencies is not evident in the hard snowball scenario, where only two peaks at 3 years and 4.3 years are evident at the 95 % confidence level. In the tropics this is similar; the hard snowball scenario shows spectral peaks at 3 and 3.3 years at the 95 % confidence level, and the equatorial oasis scenario shows spectral peaks a 3 and 4.5 years at the 95 % confidence level. In the waterbelt scenario, a much broader range of peaks between 3 and 5.6 years are evident above at least the 95 % confidence level, and peaks at 4 and 4.8 years are evident at the 99.9 % confidence level. Finally, at the Garvellach Islands, the hard snowball scenario exhibits a range of multi-annual to multidecadal peaks between 6.6 and 28.5 years at the 95 % to 99 % confidence levels. The two scenarios with open-ocean exhibit less spectral peaks at these frequencies. Spectral peak at 31.6 and 50 years are evident in the equatorial oasis scenario at the 95 % confidence level and spectral peaks at 19.3 and 26.3 years are evident in the waterbelt scenario at the 95 % and 99 % confidence levels. In the tropics, the multiannual to multidecadal peaks are less prolific, with the hard snowball scenario showing a peak at 52 years, and the equatorial oasis scenario shows a multidecadal peak of 23.5 years, both at the 99 % confidence level.

5. Discussion

The D32 laminites, we believe, provide a rare window into interannual to centennial climate dynamics during an interval of the Sturtian glaciation. By integrating sedimentological observations with fully coupled climate simulations, we develop a case below that the laminae

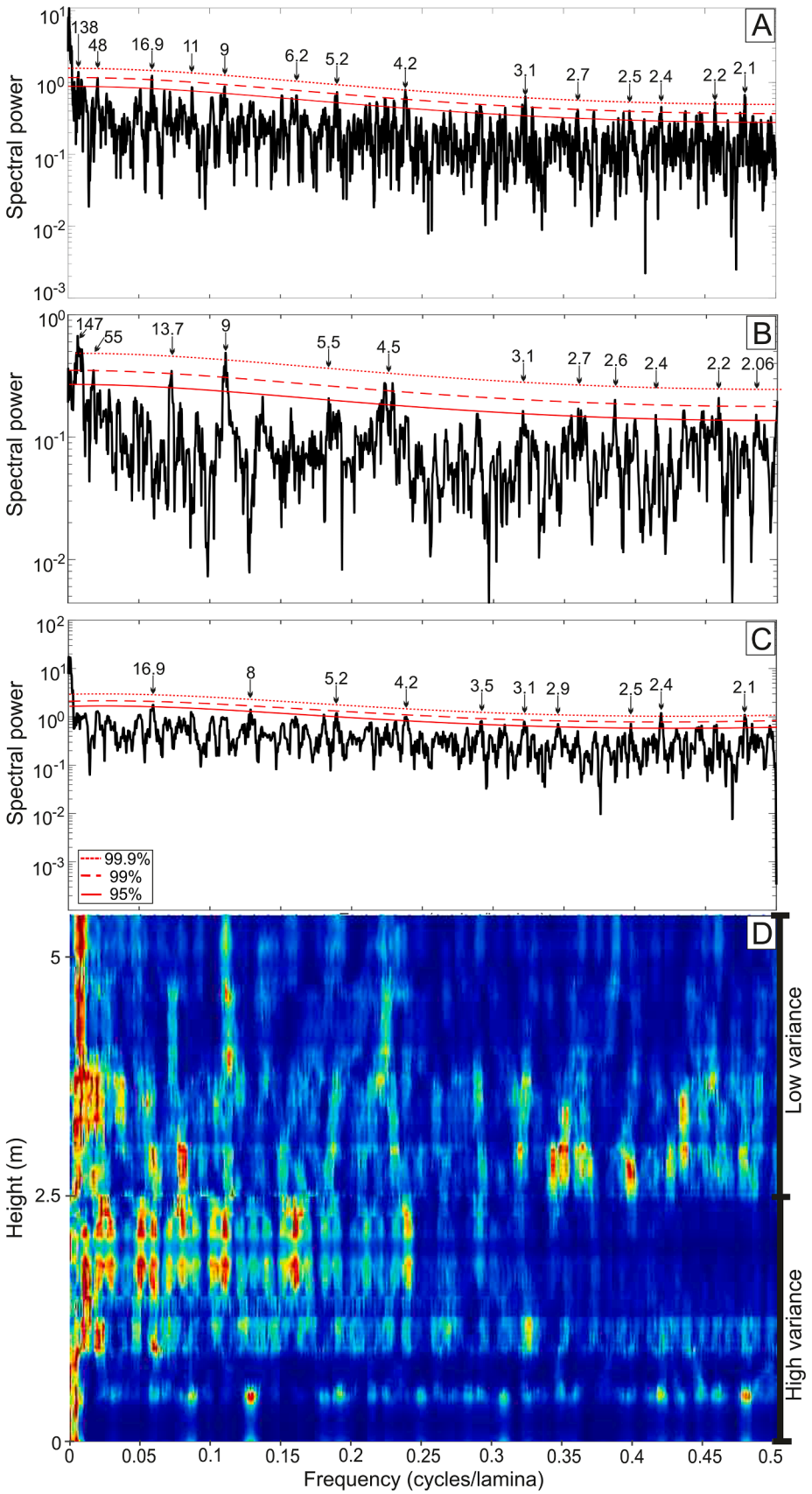

Fig. 5. Power spectra generated using the multi-taper method from the D32 laminite thickness measurements, with 95 % to 99.9 % confidence levels shown and the cycles present above the 95 % confidence level are labelled. (A) Power spectra generated from the full time series containing $n = 2{,}640$ laminae. (B) Power spectra generated from the upper half of the thickness series where variance is low ($n = 1{,}320$ laminae). (C) Power spectra generated from the lower half of the thickness series where variance is high ($n = 1{,}320$ laminae). (D) Evolutionary power spectra of the full time series.

Table 1
Summary of the signals present within the field data and the three snowball Earth simulations, both at the paleo-coordinates of the Garvellach Islands, and in an equatorial region with open tropical water.

	Field measurements (Fig. 5)			Simulation outputs from the Garvellach islands (Fig. 6)			Simulation outputs from the tropics (Fig. 7)		
	Full lamina thickness series	Upper 1320 laminae	Bottom 1320 laminae	Hard snowball scenario	Equatorial oasis scenario	Waterbelt scenario	Hard snowball scenario	Equatorial oasis scenario	Waterbelt scenario
99.9 % Confidence Level	2.1, 2.2, 3.1, 4.2	9, 147	2.1, 2.4				2.6, 2.7		2.6, 2.7, 4.0, 4.8
99 % Confidence Level	2.4, 2.5, 2.7, 5.2, 16.9, 48, 135	2.2, 2.6, 4.5, 13.7, 55		2.2, 2.3, 2.4, 2.6, 12.8	2.1, 2.5, 3.7	2.2, 2.3, 3.2, 5.2	2.3, 2.4, 52	2.0, 23.5	3.0, 3.4, 4.4, 5
95 % Confidence Level	3.2, 3.5, 4.2–2.5, 6.2–6.3, 9, 11	2.06, 2.4, 2.7, 3.1, 5.5	2.5, 2.9,3.1, 3.5, 4.2, 5.2, 8, 16.9	3.0, 4.3, 6.6, 7.7, 8.7, 28.5	2.4, 2.7, 3.2, 4.2, 5.0, 5.4, 6.0, 31.6, 50	2.5, 2.7, 3.7, 19.3, 26.3	2.1, 2.2, 3.0, 3.3	2.2, 2.4, 2.5, 3.0, 4.5	2.05, 2.1, 2.3, 2.4, 3.6, 5.3, 5.6

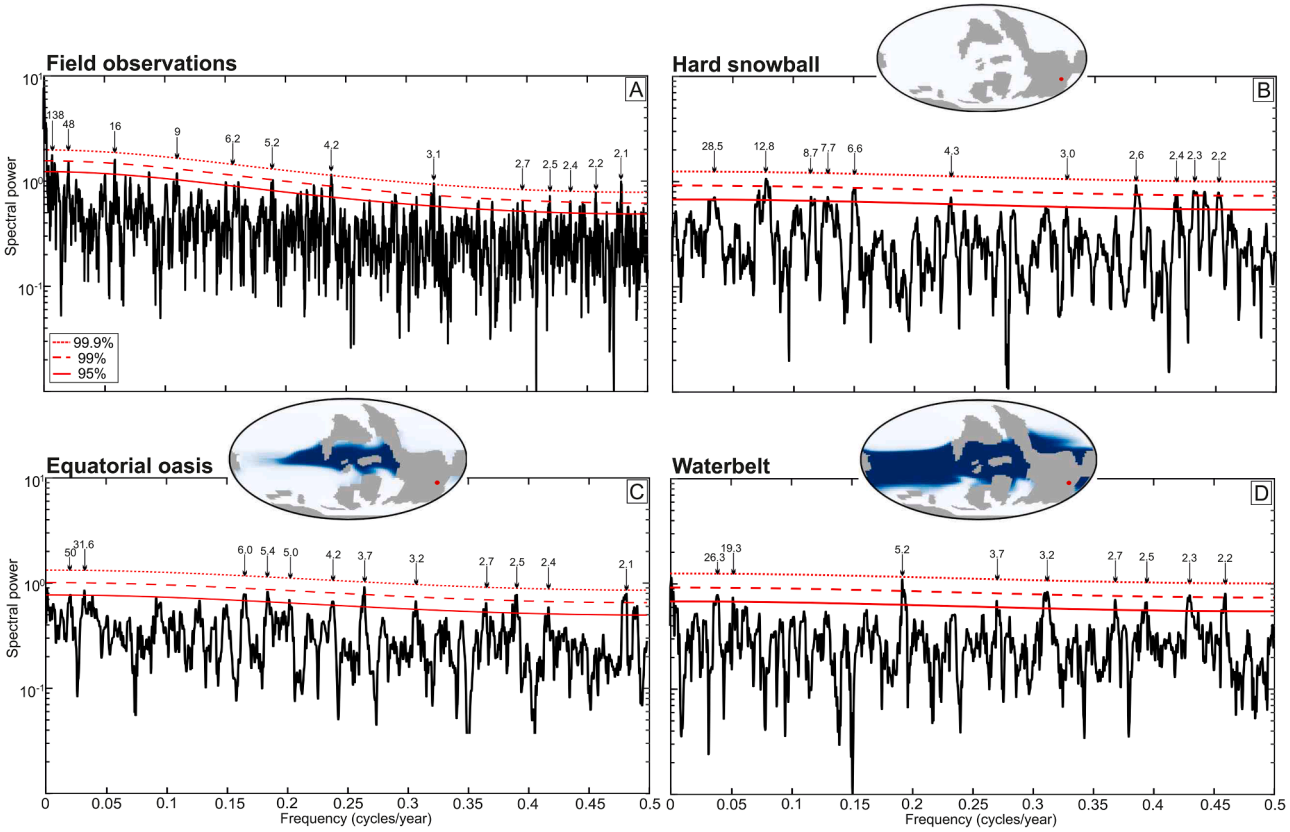

Fig. 6. Power spectra generated using the multi-taper method from simulated time series of annual surface temperature over 1000 years extracted from the paleo-coordinates of the Garvellach Islands (red dot on maps; 30.6°S, 145.6°E) for three different snowball Earth scenarios. Images above the panels denote the continental configuration (grey) and the location of ice (white) and open ocean (blue) in each scenario. (A) Power spectra from the full series of D32 laminite thickness measurements $n = 2{,}640$ laminae. (B-D) Power spectra of modelled annual temperature from the paleo-coordinates of the Garvellach Islands. (B) Hard snowball (99 % sea ice); (C) Equatorial oasis (85 % sea ice); (D) Waterbelt (60 % sea ice).

most plausibly represent annual varves deposited within a seasonally dynamic, ice-influenced glacio-lacustrine system. The strong correspondence between frequencies present in the field data and those from modelled snowball Earth climate supports the interpretation of preserved annual cyclicity modulated by solar and internal climate variability.

5.1. Origin of the laminites

Rhythmically laminated sediments can represent glacio-marine, glacio-lacustrine, sub-ice shelf or sub-glacial environments. Whilst conclusively differentiating the origin, and hence duration, of laminae can be difficult—especially in the Precambrian, (Howe et al., 2016; Livingstone et al., 2012)—several lines of evidence strongly suggest an approximately annual, ice-influenced glacio-lacustrine sedimentation pattern.

The texturally distinct light-dark couplets display plane-parallel stratification and show consistency in thicknesses throughout the outcrop (Fig. 2). Together, these two features strongly suggest formation from deposition within a conditionally motionless waterbody. Whilst differentiating tidal signatures from annual or non-annual laminations in the Precambrian record is difficult, systematic thickness variations

producing pronounced bundles of laminae typical of tidalites (e.g., Myrow et al., 2018) were not observed. Complete tidal rhythmites should record a symmetrical, continuous thick-thin alternation, with a phase flip once during each neap-spring tidal cycle (Mazumder and Arima, 2005). A lack of evidence for this persistent rhythm over the entire section leads us to infer that the individual laminae do not form part of a larger sedimentation pattern (Fig. 2B). Furthermore, whilst spectral analysis alone cannot be used to determine the origin of the laminites, the frequencies present in the field data (Fig. 5) do not align with those expected from tidal forcing (13 and 30 laminae; representing the fortnightly and monthly neap-spring tide cycle in the Neoproterozoic (Williams, 1989)), supporting a lack of tidal influence. Additionally, we do not observe sedimentary structures consistent with a marine environment or tidal influence, for example wave ripples, herringbone cross-stratification, flaser bedding, or reactivation surfaces. Whilst we acknowledge that these tidally generated sedimentary structures are not always evident, this combined with a laterally and vertically consistent lamination structure indicates an environment sheltered from wave action.

Instead, the laminations likely reflect glacio-lacustrine sedimentation in a proglacial or periglacial setting with floating ice, where they record seasonal varve formation. The occurrence of annual varves during the Cryogenian is not unreasonable due to suspected enhanced seasonality at all latitudes (Hoffman et al., 2017; Liu et al., 2020; Williams, 2008), governed by the low thermal inertia of the globally solid surface (Pierrehumbert, 2005). A sub-glacial, and therefore non-annual, origin was also considered, however in general, much thicker, coarser laminations would be expected in a directly ice-influenced location. Also, and importantly, these laminae would likely not show the vertical and lateral consistency present in the outcrop (Fig. 3). Instead, the laminae may exhibit irregular thickness in both the dark and fine layers, punctuated by erosional bases, event beds or deformation structures related to episodic drainage and pressurization events within the subglacial hydrological system (Livingstone et al., 2015, 2012)—reflecting event-driven rather than stable, predictable, annual deposition (cf. modern Antarctica; Campbell et al., 2025; Siegfried et al., 2023).

The regularity of the laminae and the presence of a dark, silt-clay layer with characteristic sharp contact with the overlying light, coarse layer is a characteristic feature of varves. This structure, paired with the variable thickness of the light layers in contrast to the independent thickness of the dark layers, forms the first basis for a varve interpretation (Palmer et al., 2019; Shatsillo et al., 2019). The lighter, coarser layers with normal grading likely represent the distal products of seasonal, quasi-continuous, sediment laden currents during the melt season, where weak internal lamination in some varves may suggest sub-seasonal currents. The thickness of the light layers therefore reflects interannual variability in melt intensity and run-off volume, driven by climatic fluctuations. In contrast, the darker, finer layers indicate uninterrupted settling of suspended loads during the non-melt season, resulting in a consistent thickness independent of summer conditions.

Further, the coarse quartz grains, which are anomalously large in relation to the host sediment and are dominant within the sand fraction of the laminae (Fig. 4, Fig. S2) are best interpreted as ice rafted debris (IRD). Whilst a solely aeolian source of these grains was considered, the sub-angularity of the grains alongside a lack of outsized sediment within the finer fraction of the laminae suggests detritus, perhaps including cryoconite (Hoffman, 2016), wind-blown onto and trapped within floating ice during the non-melt season and subsequently released during partial thawing. This is supported by the distinctive layers of outsized grains at the base of the melt-season laminae, suggestive of deposition immediately after spring thaw.

Finally, considering the underlying stratigraphy of Member 2 of the Port Askaig Formation (Fig. 1), the highly distinctive laminites form the upper unit of a 20 m sequence above an erosional incision composed of a basal conglomerate, cross-stratified sandstones, a laterally impersistent diamictite (D32) and sandstone. This sequence may reflect a periglacial incised valley fill (B. Levell, *pers. comm*), infilled by non-glacial terrestrial deposits subjected to freezing conditions—where D32 is interpreted as a non-glacial mass flow deposit—and eventually flooded by low energy standing water with floating ice (i.e., the D32 laminites). Polygonal sand wedges preserved in Member 2 of the Port Askaig Formation (Spencer, 1971) and in the top of the D32 laminites may also provide alternative geological evidence for periglacial conditions during the Sturtian. This facies sequence supports our interpretation that the laminites represent a deep, distal, ice influenced, quiet water embayment sheltered from wave action.

Taken together, the millimeter scale laminations are consistent with modern varves deposited in an intermediate to distal proglacial or periglacial lake setting, subjected to intense annual freeze-thaw events (c.f., Palmer et al., 2019). We acknowledge that other depositional rhythms could be present, or the laminae may not strictly represent annual sedimentation; for example, laminae could represent sedimentation of periods greater than one year, be absent acyclicly or may have been partially or fully eroded from the record. Whilst stratigraphic incompleteness is impossible to fully account for, sedimentation patterns radically different from an annual or other consistent pattern would present difficulties for explaining the observed regularity of the laminae or the consistency between the field data, our snowball Earth simulations (Figs. 6 and 7) and with geological observations through time (Fig. 8). Collectively, this set of constraints strengthens our confidence that the laminites record annual cyclicity.

5.2. Evidence of solar-climate interactions

The striking resemblance between the field data and the results of our new climate simulations using the paleo-location of the Garvellach Islands (Fig. 6) makes it difficult to explain the observed outcrop and spectral patterns without invoking climate influence. Whilst autocyclicity can strongly mimic external forcing, spectral analysis reveals several periodicities at the 95–99.9 % confidence levels (Fig. 5), which are consistently present even when accounting for uncertainty by applying realistic variance on the absolute thickness measurements (Fig. S1). Hence, we are confident that these represent interannual, decadal and centennial cycles reminiscent of known solar/climate oscillations. Whilst we infer a glaciolacustrine origin, we acknowledge that climatic forcing can modulate sedimentation in a variety of glacial environments capable of generating rhythmically laminated sediments. Hence, the laminites likely provide a unique, albeit transient, record of the influence of sub-Milankovitch scale forcing on glacial dynamics, irrespective of their specific depositional setting.

5.2.1. Solar cycles

The most consistent peaks within the evolutionary power spectrum occur at 9 and 130–150 laminae (Fig. 5D); such periodicities can be attributed to solar forcing, namely the decadal (c. 9–11 year) Schwabe cycle and the centennial (c. 60–150 year) Gleissberg cycle. The Schwabe cycle has been consistently documented from the Paleoproterozoic to the Holocene, with little variance in periodicity (Fig. 8). Whilst the Gleissberg cycle has been found less consistently (Tang et al., 2014), mainly due to a lack of varved records spanning multiple centuries, the long (>2600 years) varved record of the D32 laminites potentially documents ~20 Gleissberg-like cycles. The persistence and strength of these frequencies in the evolutionary power spectrum can therefore provide evidence for solar-cryosphere interactions that controlled glacial dynamics during this interval of the Sturtian.

5.2.2. Solar-climate cycles

A consistent peak within the evolutionary power spectrum also occurs at 13–16 years. Spectral peaks of 13.9, 14.3 and 17.1 laminae have been documented from varves deposited before the Sturtian and are attributed to either a long Schwabe cycle (Andrews et al., 2010) or

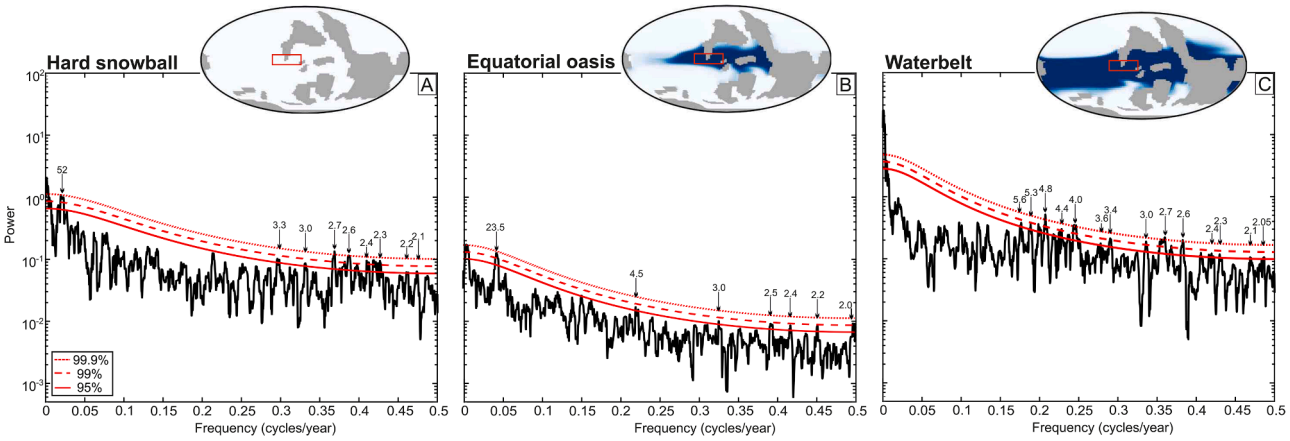

Fig. 7. Power spectra generated using the multi-taper method from simulated time series of annual surface temperature over 1000 years extracted from an equatorial region containing open tropical water in two of the scenarios (red box on maps; 5°S-5°N, 67.5°W-7.5°W) for three different snowball Earth scenarios. Images above the panels denote the continental configuration (grey) and the location of ice (white) and open ocean (blue) in each scenario. (A) Hard snowball (99 % sea ice); (B) Equatorial oasis (85 % sea ice); (C) Waterbelt (60 % sea ice).

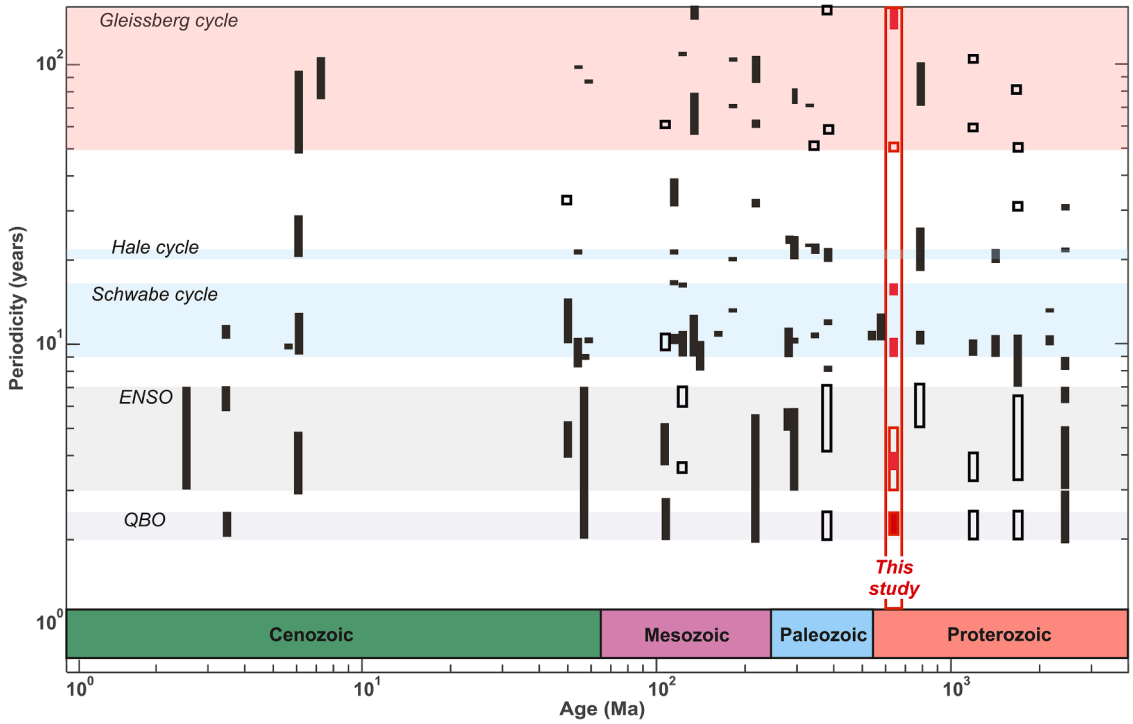

Fig. 8. Solar and climate cycles recorded in varved sediments over the last 2500 Myr, including this study (red lines). The small boxes denote the time span of the periodicities present in each study, in reference to the range of periodicities recorded for each cycle. Solid boxes denote periodicities that are consistent in multiple power spectra or stationary in an evolutionary power spectrum. Open boxes denote periodicities that are inconsistent between multiple power spectra or non-stationary in an evolutionary power spectrum. The data used to generate this figure, and their sources, are presented in Table S2.

periodic rainfall and temperature fluctuations (Hughes et al., 2003). Numerous origins for this periodicity could be explored, but the lack of similar frequencies in our climate simulations—which are run with constant solar forcing—could implicate a solar influence. The 13–16-year periodicity could be linked to the Schwabe cycle, which can increase up to 16 years during grand solar minima (Miyake et al., 2013), and may have increased due to the low solar luminosity during snowball Earth (Crowley and Baum, 1993). However, the consistency of the 9–11-year cycles reported before the Sturtian (Fig. 8), in our evolutive power spectra (Fig. 5) and in modern varves, suggest that these interactions have remained unchanged for the last ~1.2 Ga. The consistent presence of both 8–9-year and 13–16 year periodicity in the laminite thickness series may suggest the amplification of climate signals by the interaction of solar, ocean and/or atmospheric processes (Ólafsdóttir et al., 2013). Solar-ocean-atmospheric interactions can generate climatic oscillations across all frequencies (Kuroda et al., 2022), influencing global temperature and precipitation, thereby modulating sediment deposition. During snowball Earth, seasonal melting of ice sheets would have been modulated at decadal scales by solar-induced oceanographic processes (e.g., heated surface water inflow), generating dynamic ocean-atmospheric circulation patterns (Stewart et al., 2019). On the other hand, dust-cloud-surface radiation interactions can reduce surface albedo and hence drive glacial melting and increase global surface temperatures (Chen et al., 2022). Thus, these decadal cycles could

directly relate to solar-driven ocean temperature oscillations and/or wind-driven atmospheric processes, forced by solar-cryospheric-atmospheric oscillations, on decadal timescales. This suggests that solar, ocean and/or atmospheric coupling remained at least partially stable during this interval and modulated glacial dynamics and sedimentation.

5.2.3. Ocean-atmospheric climate cycles

Spectral peaks between 2 and 5 laminae appear consistently within all three power spectra but the only consistent frequency in the evolutionary power spectrum is at 4–4.5 years (Fig. 5). Therefore, these non-coherent spectral peaks may arise from short-lived, strongly periodic noise generated by stochastic sedimentation. However, spectral peaks between 2 and 6 years have been routinely documented from varves through geological time including the Precambrian (Howe et al., 2016; Hughes et al., 2003; Lafond et al., 2023; Larsen et al., 2011; Milana and Lopez, 1998; Ólafsdóttir et al., 2013; Rioja et al., 2002) (Fig. 8).

Our climate simulations from the Garvellach Islands location (Fig. 6B-D) provide evidence for spectral peaks of 2–3 years within all three climate scenarios suggesting that the non-coherent spectral peaks in the field data could arise from internal climate dynamics. Whilst the power spectra from all three scenarios display peaks between 3–6 years, the two scenarios with open-ocean display a broad range of spectral peaks above both the 95 % and 99 % confidence levels, more akin to the field data. The signals present in the power spectra from the paleolocation of the Garvellach Islands strongly agree with those from the wider ~600 km region, highlighting that the signals at this locality are unlikely to be random fluctuations (Figure S3; Supplementary Material).

In the tropics (see Fig. 7), the 4–4.5-year periodicity evident in the evolutionary power spectrum of the field data starts to emerge in the two scenarios containing open-ocean (Fig. 7). Notably, 4 year and 4.8-year periodicity is detectable at the 99.9 % confidence level in the waterbelt scenario, where full tropical ocean circulation can occur (Fig. 7C). Therefore, the tropical simulations support the view that if open-ocean existed at any time during snowball Earth, ocean-atmosphere processes similar to those of the present day were likely operating. The strong similarity between our field data, the simulations from the paleolocation of the Garvellach Islands and the simulations from the tropics suggest that the deposits may nonetheless preserve episodic manifestations of this variability. This is especially highlighted by the consistent 4-year periodicity evident in the evolutionary power spectrum and in the simulated power spectra of the tropics. Hence, these non-stationary, interannual signals could be intrinsic to snowball Earth climate dynamics and may arise from QBO-like and ENSO-like oscillations which both exhibit clear signatures in temperature and pressure, influencing the intensity and duration of ice melt (Baldwin et al., 2001). As the average periodicity of the modern ENSO is ~4 years, the consistency of the 4 and 16-year periodicities may further indicate the presence of both the high and low frequency components of climate modes (c.f. the Pacific Decadal Oscillation; a prolonged ENSO-like pattern). Together, these observations hint at an interval of dynamic interannual climate variability during the Sturtian that is reminiscent of other periods of Earth history (Davies et al., 2011; Gao et al., 2025)

5.2.4. Constraints from previous and new climate models

Crucially, under a totally ice-covered scenario, it is unlikely that climatic variations dependent on air-sea interactions over large sections of open ocean (e.g., ENSO) would continue to operate. Modelling studies have shown that in a hard snowball scenario, geothermal heat flux and surface ice melting can generate vigorous ocean circulation patterns at many frequencies (Ashkenazy et al., 2014; Ashkenazy and Tziperman, 2016), but it is unlikely that an expression of this ocean variability would be seen above kilometer-thick ice. This makes the inferences of snowball Earth climatic variability at interannual timescales found in this study particularly surprising.

Comparison of annual surface temperature in the tropics in the simulated scenarios (Fig. 7) may provide evidence that the interannual oscillations can be attributed to, and hence document the operation of, climate modes similar to those of the modern day in the Cryogenian. The consistency of 2–3-year frequencies in all three modelled scenarios allows the inference of a QBO-like climate mode, which does not require air-sea interaction and hence would be expected to continue even under hard snowball Earth conditions. In our models, climatic variability in the hard snowball scenario is dominated by biennial oscillations (Fig. 7A), which due to a near entirely frozen ocean, is likely the only climate mode (besides solar forcing) able to operate and influence glacial dynamics.

In the tropics, the waterbelt scenario (Fig. 7C) strongly documents the familiar quasi-periodic 3–7-year frequencies reminiscent of the modern ENSO. Whilst the intensity of air-sea interactions undoubtedly varied due to paleogeographic changes, the extent of ice coverage, and much colder global temperatures, these periodicities are similar to those of the modern day. Any Earth climate state with some degree of open-ocean should generate air-sea interactions over interannual timescales, as previously documented in the modern icehouse and previous greenhouse climates (Gao et al., 2025). The evolutionary power spectrum of our field data supports the existence of a 4–4.5-year periodicity, which is evident in the tropics in both scenarios containing partially open-ocean (Fig. 7). The apparent increased strength of the 4–4.5-year periodicity in the tropics as the amount of open-ocean increases (Figs. 7B and C) may document more established air-sea interactions on snowball Earth as the scale of ocean circulation increases. Hence, our simulations point towards the existence of these interactions in snowball Earth states that contain over 1 % open-ocean. Whilst the hard snowball scenario does contain peaks at 3 and 3.3 years, the broad range of peaks documenting the non-stationarity of this signal is not present—particularly the ~4 year periodicity observed in our field data and in the two open-ocean scenarios. Therefore, these periodicities are likely linked either to stochastic noise or to the upper limit of the QBO-like oscillation.

Comparison of the power spectra of our field data to those from our climate simulations (Figs. 6 and 7) point towards an interval of dynamic climate variability driven by solar-ocean-atmospheric exchanges, only viable in a scenario lacking a completely sealed snowball ocean. Given the evidence that the signals in the field data reflect genuine climate variability, our simulations favor a transient “slushball” or “waterbelt” scenario. This interpretation implies the existence of localized, ice-free topical waters during this discrete ~2500-year interval of the Sturtian glaciation. Intriguingly, several lines of evidence suggest that a partially ice-free ocean existed for a similar phase of the Sturtian (Lan et al., 2022 and references therein). Hence, these laminites may provide further sedimentological evidence for remarkably transient open-ocean conditions during this interval. Moreover, the scarcity of laminated rhythmites across most of the Cryogenian Period may even support the existence of a largely “hard” long-lived Sturtian snowball Earth. Irrespective of the mechanism driving such conditions, our simulations indicate that even restricted open-water regions can permit solar-ocean-atmospheric interactions, generating a much wider range of climatic variability than expected under snowball Earth conditions.

6. Conclusions

The D32 laminites in the Port Askaig Formation are interpreted as annual varves, recording seasonal freeze-thaw processes in a low energy, standing water body with floating ice, sheltered from wave action. This interpretation supports the existence of an active hydrological cycle during at least part of the Sturtian. Assuming annual sedimentation, spectral analysis reveals the stability and persistence of interannual to centennial climatic variability, with similar periodicities to modern solar and climatic oscillations, which have not been documented previously during the Cryogenian. Decadal to centennial periodicities of strong similarity to solar phenomena, and interannual periodicities similar to modern ocean-atmospheric climate patterns, suggest either a

discrete interval of open tropical water during the Sturtian or yet unexplored mechanisms of interannual variability on icy worlds. Such findings are consistent with new fully coupled snowball Earth climate simulations in which open water is present in the tropics during the Sturtian glaciation. The persistence of both solar and climatic oscillations could hint that solar-induced oceanographic processes influenced regional climates, surface temperatures and seasonal melting of ice sheets on timescales akin to the present day. Our findings may indicate a climatic episode during the Sturtian, during which transient open-ocean conditions occurred, pointing to a wider range of climatic variability than previously envisaged during snowball Earth.

CRediT authorship contribution statement

Chloe Griffin: Writing – review & editing, Writing – original draft, Visualization, Validation, Methodology, Investigation, Formal analysis, Data curation, Conceptualization. **Thomas M. Gernon:** Writing – review & editing, Visualization, Supervision, Resources, Project administration, Methodology, Funding acquisition, Conceptualization. **Minmin Fu:** Writing – review & editing, Validation, Software, Resources, Methodology, Investigation, Formal analysis, Data curation. **Elias J. Rugen:** Writing – review & editing, Visualization, Resources, Investigation, Conceptualization. **Anthony M. Spencer:** Writing – review & editing, Resources, Methodology, Conceptualization. **Geoffrey Warrington:** Writing – review & editing, Resources, Investigation. **Thea K. Hincks:** Writing – review & editing, Validation, Software, Formal analysis.

Declaration of competing interest

The authors declare that they have no known competing financial interests or personal relationships that could have appeared to influence the work reported in this paper.

Acknowledgements

We gratefully acknowledge funding from the WoodNext Foundation, a fund of a donor-advised fund program. We thank Paul Hoffman and Bruce Levell for helpful discussion and insightful comments which helped shape some of the interpretations in this paper. We acknowledge constructive reviews by Camille Partin, Thomas Vandyk and other anonymous reviewers. We also thank Ninian Johnson-Ferguson, Becky Weatherley and Alasdair MacLachlan for their hospitality and expert boat services in and around the Garvellach Islands.

Supplementary materials

Supplementary material associated with this article can be found in the online version, at doi:10.1016/j.epsl.2026.119891.

Data availability

Data will be made available on request.

References

Abbot, D.S., Voigt, A., Koll, D., 2011. The Jormungand global climate state and implications for Neoproterozoic glaciations. J. Geophys. Res. Atmos. https://doi.org/10.1029/2011JD015927.

Ali, D.O., Spencer, A.M., Fairchild, I.J., Chew, K.J., Anderton, R., Levell, B.K., Hambrey, M.J., Dove, D., Le Heron, D.P., 2018. Indicators of relative completeness of the glacial record of the Port Askaig Formation, Garvellach Islands, Scotland. Precambrian. Res. 319, 65–78. https://doi.org/10.1016/j.precamres.2017.12.005.

Amann, B., Szidat, S., Grosjean, M., 2015. A millennial-long record of warm season precipitation and flood frequency for the North-western Alps inferred from varved lake sediments: implications for the future. Quat. Sci. Rev. 115, 89–100. https://doi.org/10.1016/j.quascirev.2015.03.002.

Andrews, S.D., Trewin, N.H., Hartley, A.J., Weedon, G.P., 2010. Solar variance recorded in lacustrine deposits from the Devonian and Proterozoic of Scotland. J. Geol. Soc. London. 167, 847–856. https://doi.org/10.1144/0016-76492009-105.

Antoniazza, G., Lane, S.N., 2021. Sediment yield over glacial cycles: a conceptual model. Prog. Phys. Geogr. 45, 842–865. https://doi.org/10.1177/0309133321997292.

Ashkenazy, Y., Gildor, H., Losch, M., Tziperman, E., 2014. Ocean circulation under globally glaciated snowball earth conditions: steady-state solutions. J. Phys. Oceanogr. 44, 24–43. https://doi.org/10.1175/JPO-d-13-086.1.

Ashkenazy, Y., Tziperman, E., 2016. Variability, instabilities, and eddies in a snowball ocean. J. Clim. 29, 869–888. https://doi.org/10.1175/JCLI-d-15-0308.1.

Baldwin, M.P., Gray, L.J., Dunkerton, T.J., Hamilton, K., Haynes, P.H., Randel, W.J., Holton, J.R., Alexander, M.J., Hirota, I., Horinouchi, T., Jones, D.B.A., Kinnersley, J. S., Marquardt, C., Sato, K., Takahashi, M., 2001. The quasi-biennial oscillation. Rev. Geophys. 39, 179–229. https://doi.org/10.1029/1999RG000073.

Benn, D.I., Le Hir, G., Bao, H., Donnadieu, Y., Dumas, C., Fleming, E.J., Hambrey, M.J., McMillan, E.A., Petronis, M.S., Ramstein, G., Stevenson, C.T.E., Wynn, P.M., Fairchild, I.J., 2015. Orbitally forced ice sheet fluctuations during the Marinoan Snowball Earth glaciation. Nat. Geosci. 8, 704–707. https://doi.org/10.1038/ngeo2502.

Brauer, A., 2004. Annually laminated lake sediments and their palaeoclimatic relevance. The Climate in Historical Times; GKSS School of Environmental Research. Springer, Berlin/Heidelberg, Germany, pp. 109–127.

Campbell, T.D., Skidmore, M.L., Patterson, M.O., Dore, J.E., Harwood, D.M., Leventer, A., Michaud, A.B., Rosenheim, B.E., Siegfried, M.R., Steigmeyer, A.J., Tranter, M., Venturelli, R.A., Priscu, J.C., 2025. Dynamic subglacial meltwater history archived in Antarctic subglacial lake sediments. Bull. Geol. Soc. Am. 137, 3055–3068. https://doi.org/10.1130/B37731.1.

Chen, S., Bi, H., Zhang, R., Wang, Y., Guo, J., Zhao, D., Chen, Y., Guan, Y., Xie, Z., 2022. Impact of dust-cloud-radiation interactions on surface albedo: a case study of "Tiramisu" snow in Urumqi, China. Environ. Res. Lett. 17. https://doi.org/10.1088/1748-9326/ac3b18.

Crowley, T.J., Baum, S.K., 1993. Effect of decreased solar luminosity on late precambrian ice extent. J. Geophys. Res. 98. https://doi.org/10.1029/93jd01415.

Danabasoglu, G., Bates, S.C., Briegleb, B.P., Jayne, S.R., Jochum, M., Large, W.G., Peacock, S., Yeager, S.G., 2012. The CCSM4 ocean component. J. Clim. 25, 1361–1389. https://doi.org/10.1175/JCLI-d-11-00091.1.

Davies, A., Kemp, A.E.S., Pälike, H., 2011. Tropical ocean-atmosphere controls on interannual climate variability in the Cretaceous Arctic. Geophys. Res. Lett. 38. https://doi.org/10.1029/2010GL046151.

De Geer, G., 1912. A geochronology of the last 12000 years. In: Compte Rendu 11 Congress Geologique International, 11th International Geological Congress (1910), Stockholm, Sweden, pp. 241–253 vol. 1.

De Geer, G., 1908. On late quaternary time and climate. Geol. Föreningen Stock, Förhandlingar 30, 459–464.

Dean, W., Anderson, R., Bradbury, J.P., Anderson, D., 2002. A 1500-year record of climatic and environmental change in Elk Lake, Minnesota I: varve thickness and gray-scale density. J. Paleolimnol. 27, 287–299.

Deynoux, M., 1982. Periglacial polygonal structures and sand wedges in the late precambrian glacial formations of the taoudeni basin in Adrar of Mauretania (West Africa). Palaeogeogr. Palaeoclimatol. Palaeoecol. 39, 55–70.

Fairchild, I.J., Spencer, A.M., Ali, D.O., Anderson, R.P., Anderton, R., Boomer, I., Dove, D., Evans, J.D., Hambrey, M.J., Howe, J., Sawaki, Y., Shields, G.A., Skelton, A., Tucker, M.E., Wang, Z., Zhou, Y., 2018. Tonian-cryogenian boundary sections of Argyll, Scotland. Precambrian. Res. 319, 37–64. https://doi.org/10.1016/j.precamres.2017.09.020.

Gao, Y., Tian, X., Hu, Y., Li, X., Cai, W., Qin, J., Guo, J., Du, X., Kukla, T., Ibarra, D.E., Huang, H., Wu, L., Wang, C., 2025. Active El Niño–Southern Oscillation–like interannual variability 120 million years ago. Geology. https://doi.org/10.1130/G53646.1.

Hasegawa, H., Katsuta, N., Muraki, Y., Heimhofer, U., Ichinnorov, N., Asahi, H., Ando, H., Yamamoto, K., Murayama, M., Ohta, T., Yamamoto, M., Ikeda, M., Ishikawa, K., Kuma, R., Hasegawa, T., Hasebe, N., Nishimoto, S., Yamaguchi, K., Abe, F., Tada, R., Nakagawa, T., 2022. Decadal–centennial-scale solar-linked climate variations and millennial-scale internal oscillations during the early Cretaceous. Sci. Rep. 12. https://doi.org/10.1038/s41598-022-25815-w.

Hoffman, P.F., 2016. Cryoconite pans on Snowball Earth: supraglacial oases for Cryogenian eukaryotes? Geobiology 14, 531–542. https://doi.org/10.1111/gbi.12191.

Hoffman, P.F., Abbot, D.S., Ashkenazy, Y., Benn, D.I., Brocks, J.J., Cohen, P.A., Cox, G. M., Creveling, J.R., Donnadieu, Y., Erwin, D.H., Fairchild, I.J., Ferreira, D., Goodman, J.C., Halverson, G.P., Jansen, M.F., Le Hir, G., Love, G.D., Macdonald, F. A., Maloof, A.C., Partin, C.A., Ramstein, G., Rose, B.E.J., Rose, C.V., Peter, S.M., Tziperman, E., Voigt, A., Warren, S.G., 2017. Snowball Earth climate dynamics and Cryogenian geology-geobiology. Sci. Adv. 3, e1600983. https://doi.org/10.1126/sciadv.1600983.

Hoffman, P.F., Kaufman, A.J., Halverson, G.P., Schrag, D.P., 1998. A Neoproterozoic Snowball Earth. Science 281, 1342–1346. https://doi.org/10.1126/science.281.5381.1342.

Hoffman, P.F., Li, Z.X., 2009. A palaeogeographic context for Neoproterozoic glaciation. Palaeogeogr. Palaeoclimatol. Palaeoecol. 277, 158–172. https://doi.org/10.1016/j.palaeo.2009.03.013.

Howe, T.S., Corcoran, P.L., Longstaffe, F., Webb, E.A., Gerhard Pratt, R., Gerhard, R., 2016. Climatic cycles recorded in glacially influenced rhythmites of the Gowganda formation. Huronian Supergr., Earth Sci. Publ. 16.

Huber, M., Caballero, R., 2003. Eocene El Niño: evidence for robust tropical dynamics in the "hothouse". Science 299, 877–881. https://doi.org/10.1126/science.1078766.

Hughes, G.B., Giegengack, R., Kritikos, H.N., 2003. Modern spectral climate patterns in rhythmically deposited argillites of the Gowganda Formation (Early Proterozoic), southern Ontario. Canada. Earth Planet. Sci. Lett. 207, 13–22. https://doi.org/10.1016/S0012-821X(02)01155-X.

Hyde, W.T., Crowley, T.J., Baum, S.K., Peltier, W.R., 2, 2000. Neoproterozoic `snowball Earth' simulations with a coupled climate/ice-sheet model. Nature 405, 425-429, doi:10.1038/35013005.

Korn, H., Martin, H., 1951. Cyclic sedimentation in varved sediments of the Nama system in South-West Africa. S. Afr. J. Geol. 54, 65–67.

Kuroda, Y., Kodera, K., Yoshida, K., Yukimoto, S., Gray, L., 2022. Influence of the solar cycle on the North Atlantic oscillation. J. Geophys. Res.: Atmos. 127. https://doi.org/10.1029/2021JD035519.

Lafond, K.M., Walsh, C.R., Patterson, R.T., McCarthy, F.M.G., Llew-Williams, B.M., Hamilton, P.B., Nasser, N.A., Cumming, B., 2023. Influence of climatic trends and cycles on varve deposition in Crawford Lake, Ontario, Canada. Geosciences. (Basel) 13. https://doi.org/10.3390/geosciences13030087.

Lan, Z., Mitchell, R.N., Gernon, T.M., Nordsvan, A.R., 2022. Did an asteroid impact cause temporary warming during snowball Earth? Earth. Planet. Sci. Lett. 581. https://doi.org/10.1016/j.epsl.2022.117407.

Larsen, D.J., Miller, G.H., Geirsdóttir, Á., Thordarson, T., 2011. A 3000-year varved record of glacier activity and climate change from the proglacial lake Hvítárvatn. Iceland. Quat. Sci. Rev. 30, 2715–2731. https://doi.org/10.1016/j.quascirev.2011.05.026.

Le Heron, D.P., Cox, G., Trundley, A., Collins, A., 2011. Sea ice−free conditions during the Sturtian glaciation (early Cryogenian), South Australia. Geology. 39, 31–34.

Li, M., Hinnov, L., Kump, L., 2019. Acycle: time-series analysis software for paleoclimate research and education. Comput. Geosci. 127, 12–22. https://doi.org/10.1016/j.cageo.2019.02.011.

Li, P., Tang, D., Shi, X., Jiang, G., Zhao, X., Zhou, X., Wang, X., Chen, X., 2018. Sunspot cycles recorded in siliciclastic biolaminites at the dawn of the Neoproterozoic Sturtian glaciation in South China. Precambrian. Res. 315, 75–91. https://doi.org/10.1016/j.precamres.2018.07.018.

Li, X., Hu, S., Hu, Y., Cai, W., Jin, Y., Lu, Z., Guo, J., Lan, J., Lin, Q., Yuan, S., Zhang, J., Wei, Q., Liu, Y., Yang, J., Nie, J., 2024. Persistently active El Niño–Southern oscillation since the Mesozoic. Proc. Natl. Acad. Sci. U. S. A. 121. https://doi.org/10.1073/pnas.2404758121.

Liu, Y., Yang, J., Bao, H., Shen, B., Hu, Y., 2020. Large equatorial seasonal cycle during Marinoan snowball Earth. Sci. Adv. 6, eaay2471. https://doi.org/10.1126/sciadv.aay2471.

Livingstone, S.J., Clark, C.D., Piotrowski, J.A., Tranter, M., Bentley, M.J., Hodson, A., Swift, D.A., Woodward, J., 2012. Theoretical framework and diagnostic criteria for the identification of palaeo-subglacial lakes. Quat. Sci. Rev. 53, 88–110. https://doi.org/10.1016/j.quascirev.2012.08.010.

Livingstone, S.J., Piotrowski, J.A., Bateman, M.D., Ely, J.C., Clark, C.D., 2015. Discriminating between subglacial and proglacial lake sediments: an example from the Dänischer Wohld Peninsula, northern Germany. Quat. Sci. Rev. 112, 86–108. https://doi.org/10.1016/j.quascirev.2015.01.030.

Mazumder, R., Arima, M., 2005. Tidal rhythmites and their implications. Earth. Sci. Rev. 69, 79–95. https://doi.org/10.1016/j.earscirev.2004.07.004.

McPhaden, M.J., Zebiak, S.E., Glantz, M.H., 2006. ENSO as an Integrating Concept in Earth Science. Science 314 (5806), 1740–1745. https://doi.org/10.1126/science1132588.

Merdith, A.S., Williams, S.E., Collins, A.S., Tetley, M.G., Mulder, J.A., Blades, M.L., Young, A., Armistead, S.E., Cannon, J., Zahirovic, S., Müller, R.D., 2021. Extending full-plate tectonic models into deep time: linking the Neoproterozoic and the Phanerozoic. Earth. Sci. Rev. 214, 103477. https://doi.org/10.1016/j.earscirev.2020.103477.

Milana, J.P., Lopez, S., 1998. Solar Cycles Recorded in Carboniferous glacimarine Rhythmites (Western Argentina): Relationships between Climate and Sedimentary Environment. Palaeoecology, Palaeoclimatology.

Mitchell, R.N., Gernon, T.M., Cox, G.M., Nordsvan, A.R., Kirscher, U., Xuan, C., Liu, Y., Liu, X., He, X., 2021. Orbital forcing of ice sheets during snowball Earth. Nat. Commun. 12. https://doi.org/10.1038/s41467-021-24439-4.

Miyake, F., Masuda, K., Nakamura, T., 2013. Lengths of Schwabe cycles in the seventh and eighth centuries indicated by precise measurement of carbon-14 content in tree rings. J. Geophys. Res. Space Phys. 118, 7483–7487. https://doi.org/10.1002/2012JA018320.

Myrow, P.M., Lamb, M.P., Ewing, R.C., 2018. Rapid sea level rise in the aftermath of a Neoproterozoic snowball Earth. Science 360 (6389), 649–651. https://doi.org/10.1126/science.aap8612.

Neale, R.B., Gettelman, A., Park, S., Chen, C.-C., Lauritzen, P.H., Williamson, D.L., Conley, A.J., Kinnison, D., Marsh, D., Smith, A.K., Vitt, F., Garcia, R., Lamarque, J.-F., Mills, M., Tilmes, S., Morrison, H., Cameron-Smith, P., Collins, W.D., Iacono, M. J., Easter, R.C., Liu, X., Ghan, S.J., Rasch, P.J., Taylor, M.A., 2012. Description of the NCAR Community atmosphere model (CAM 5.0). NCAR Tech. Note NCAR/TN-486 + STR.

Ojala, A.E.K., Francus, P., Zolitschka, B., Besonen, M., Lamoureux, S.F., 2012. Characteristics of sedimentary varve chronologies - a review. Quat. Sci. Rev. 43, 45–60. https://doi.org/10.1016/j.quascirev.2012.04.006.

Ólafsdóttir, K.B., Geirsdóttir, Á., Miller, G.H., Larsen, D.J., 2013. Evolution of NAO and AMO strength and cyclicity derived from a 3-ka varve-thickness record from Iceland. Quat. Sci. Rev. 69, 142–154. https://doi.org/10.1016/j.quascirev.2013.03.009.

Palmer, A.P., Bendle, J.M., MacLeod, A., Rose, J., Thorndycraft, V.R., 2019. The micromorphology of glaciolacustrine varve sediments and their use for reconstructing palaeoglaciological and palaeoenvironmental change. Quat. Sci. Rev. 226. https://doi.org/10.1016/j.quascirev.2019.105964.

Pierrehumbert, R.T., 2005. Climate dynamics of a hard snowball Earth. J. Geophys. Res. D: Atmos. 110, 1–22. https://doi.org/10.1029/2004JD005162.

Reid, G.C., 2000. Solar variability and the Earth's climate: introduction and overview. Space Sci. Rev. 94, 1–11.

Rioja, L., Munoz, A., Ojeda, J., Sanchez-Valverde, B., 2002. Sunspot-like and ENSO /NAO-like periodicities in lacustrine laminated sediments of the pliocene Villarroya Basin. J. Paleolimnol. 27, 453–463.

Rugen, E.J., Pastore, G., Vermeesch, P., Spencer, A.M., Webster, D., Smith, A.G.G., Carter, A., Shields, G.A., 2024. Glacially influenced provenance and sturtian affinity revealed by detrital zircon U-Pb ages from sandstones in the Port Askaig Formation. Dalradian Supergroup. J. Geol. Soc. London. 181 (5), jgs2024–029. https://doi.org/10.1144/jgs2024-029.

Shatsillo, A.V., Rud'ko, S.V., Latysheva, I.V., Rud'ko, D.V., Fedyukin, I.V., Malyshev, S. V., 2019. Paleomagnetic, sedimentological, and isotopic data on Neoproterozoic periglacial sediments of Siberia: a new perspective on the low-latitude glaciations problem. Izvestiya. Phys. Solid Earth 55, 841–863. https://doi.org/10.1134/S1069351319060065.

Siegfried, M.R., Venturelli, R.A., Patterson, M.O., Arnuk, W., Campbell, T.D., Gustafson, C.D., Michaud, A.B., Galton-Fenzi, B.K., Hausner, M.B., Holzschuh, S.N., Huber, B., Mankoff, K.D., Schroeder, D.M., Summers, P.T., Tyler, S., Carter, S.P., Fricker, H.A., Harwood, D.M., Leventer, A., Rosenheim, B.E., Skidmore, M.L., Priscu, J.C., 2023. The life and death of a subglacial lake in West Antarctica. Geology. 51, 434–438. https://doi.org/10.1130/G50995.1.

Spencer, A.M., 1971. The late Precambrian glaciation in Scotland. Geological Society, London. Memoirs 6, 5–102.

Stewart, A.L., Klocker, A., Menemenlis, D., 2019. Acceleration and overturning of the antarctic slope current by winds, eddies, and tides. J. Phys. Oceanogr. 49, 2043–2074. https://doi.org/10.1175/JPO-d-18-0221.1.

Tang, D., Shi, X., Jiang, G., 2014. Sunspot cycles recorded in mesoproterozoic carbonate biolaminites. Precambrian. Res. 248, 1–16. https://doi.org/10.1016/j.precamres.2014.04.009.

Thomson, D.J., 1982. Spectrum estimation and harmonic analysis. Proc. IEEE 70.

Usoskin, I.G., Mursula, K., 2003. Long-term solar cycle evolution: review of recent developments. Sol. Phys. 218, 319–343.

Van De Koot, E.K., Byrne, M.P., Woollings, T., 2025. Tropical cloud feedbacks estimated from observed multidecadal trends. J. Clim. 38, 3185–3199. https://doi.org/10.1175/JCLI-d-24.

Weedon, G., 2003. Time-Series Analysis and Cyclostratigraphy: Examining stratigraphic Records of Environmental Cycles. Cambridge University Press.

Weedon, G.P., Page, K.N., Jenkyns, H.C., 2019. Cyclostratigraphy, stratigraphic gaps and the duration of the Hettangian Stage (Jurassic): insights from the Blue Lias Formation of southern Britain. Geol. Mag. 156, 1469–1509. https://doi.org/10.1017/S0016756818000808.

Williams, G.E., 2008. Proterozoic (pre-Ediacaran) glaciation and the high obliquity, low-latitude ice, strong seasonality (HOLIST) hypothesis: principles and tests. Earth. Sci. Rev. 87, 61–93. https://doi.org/10.1016/j.earscirev.2007.11.002.

Williams, G.E., 1989. Late Precambrian tidal rhythmites in South Australia and the history of the Earth's rotation. J. Geol. Soc. London. 146, 97–111.

Zolitschka, B., Francus, P., Ojala, A.E.K., Schimmelmann, A., 2015. Varves in lake sediments - a review. Quat. Sci. Rev. 117, 1–41. https://doi.org/10.1016/j.quascirev.2015.03.019.